國立臺灣大學理學院應用物理研究所

碩士論文

Graduate Institute of Applied Physics

College of Science

National Taiwan University

Master Thesis

回音廊模態增強氧化鋅奈米柱的隨機雷射

Enhancement of Random Laser Action Assisted by

Whispering-Gallery-Mode Resonance

翁桐敏

Tong-Ming Weng

指導教授：陳永芳 博士

Advisor: Yang-Fang Chen, Ph.D.

中華民國 102 年 7 月

July, 2013

摘要

本論文主要目的在於研究利用回音廊模態增強氧化鋅奈米柱的隨機雷射。為了探討其中的運作原理，我們研究了二氧化矽奈米球修飾氧化鋅奈米線的雷射特性。我們發現在二氧化矽奈米球的幫助下，放射光譜裡有數個半高寬小於 0.3 奈米的雷射尖峰，而隨機雷射的微分量子效率也增加了七倍。拿來做修飾的奈米球不但可以做為回音廊模態的共振腔、增強發光強度，也可以做為一個散射中心。透過我們元件的二維的陰極發光影像、圓形迴音廊模態的理論計算、不同大小氧化矽奈米球的使用，我們進一步地驗證了提出的理論。這樣獨特的雷射特性將可以利用在製作高效率的光電元件。

Abstract

Whispering-gallery-mode (WGM) resonance enhanced random laser action has been proposed and demonstrated. To illustrate the working principle, lasing characteristics of ZnO nanorods decorated with SiO_2 nanospheres have been investigated. It is found that with the assistance of SiO_2 nanospheres, the emission spectrum exhibits a very narrow background signal with few sharp lasing peaks and a very small full width at half maximum of less than 0.3 nm. The differential quantum efficiency (η_d) of random laser action can be greatly enhanced by up to 735 %. The decorated nanospheres not only enable to generate WGM resonance and enhance the emission intensity, but also can serve as scattering centers. Cathodoluminescence mapping images of nanorods decorated with nanospheres and theoretical calculation based on the spherical cavity were utilized to confirm our proposed mechanism. The unique lasing behavior shown here may open up a new approach for the creation of highly efficient optoelectronic devices.
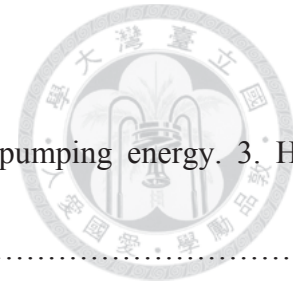
Contents

List of Figures and Tables

Chapter 1

Introduction

Laser, as shown in Fig 1.1, which is usually constructed from a material that provides optical gain through stimulated emission and an optical cavity that partially traps the light. Once the total gain in this cavity is larger than losses, the system reaches a threshold and begin lasing. Over the past decade, the random amplifying medium which has been a topic of intense research. Mutiple scattering in disordered optical materials is complex yet completely coherent, which means that the phase of each of the optical wavelets undergoing a random walk is well defined and interference effects can occur, even if a material is strongly disordered. Finally, laser physics and mutiple scattering meet in the random laser : a mutiple scattering medium amplifies light to reach a lasing threshold as shown in Fig 1.2.
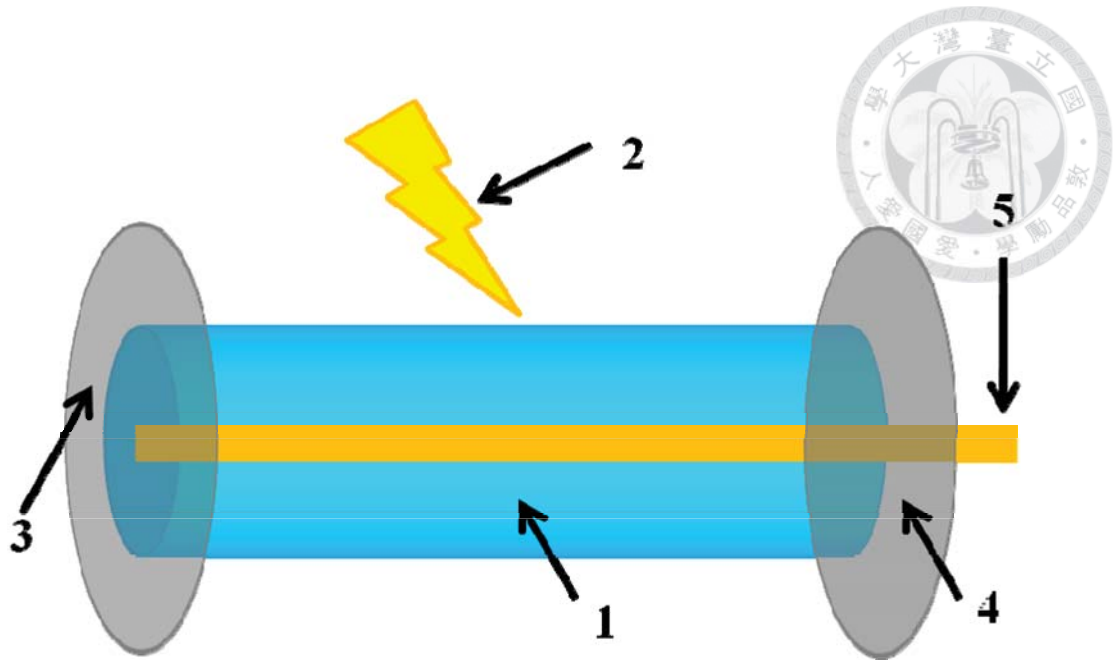
Fig. 1.1 Components of a typical laser: 1. Gain medium.
2. Laser pumping energy. 3. High reflector 4. Output
coupler 5. Laser beam.

In 1968, Letokhov[1] theoretically predicted that laser-like emission from amplifying

disordered materials can be obtained by using non-resonant positive feedback via

multiple scattering of light. Unlike with the conventional laser action via Fabry-Perot

resonance, random laser cavities are self-formed to achieve coherent feedback in the

laser system with its low-cost and simple process technology. Moreover, random lasing

usually exhibits a very broad angular distribution which is ideal for display application.
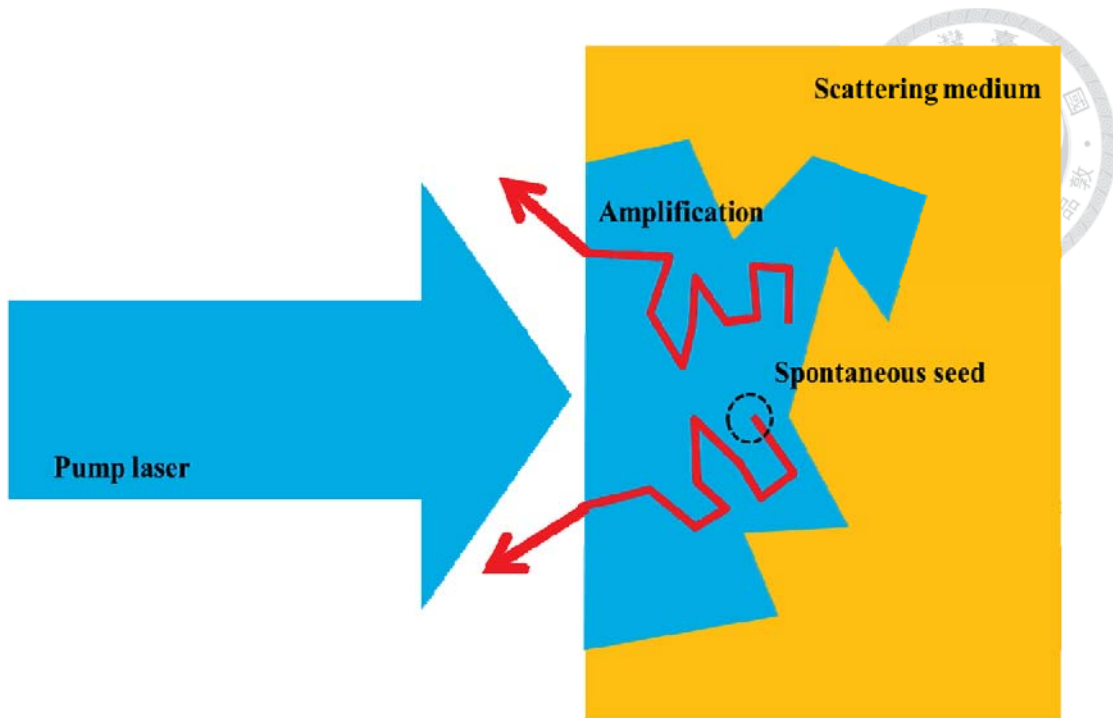
Fig. 1.2 Schematic representation of a random laser.

So far, random lasing action has been found in many kinds of media such as inorganic semiconductors, organic molecules, biological systems and cold atoms.[2-5] It has also been widely studied in nanoscale materials such as nanorod arrays and nanocrystalline films.[6,7] ZnO, with a wide bandgap of 3.37 eV , a high exciton binding energy of 60 meV, and plenty kinds of nanostructures, is very suitable for the fabrication of ultraviolet light-emitting diodes and laser devices with high efficiency.[8-10] In addition, due to a high refractive index in ultraviolet region ($\sim$ 2.5), the total internal reflection in ZnO structures can be easily achieved. Based on these favorable properties, conventional laser actions from ZnO nanostructures have been successfully demonstrated by many types of resonators.[11-13] However, according to previous

studies,[14] the emission of ZnO nanorods (NRs) fabricated by vapor-solid (VS) growth

mechanism only shows a very broad spectrum which means random laser action still

needs improvement .[7,15]

Encouraged by the above mentioned novel properties arising from nanoscale

materials, in this thesis, we provide an alternative approach to enhance the random

lasing behavior arising from VS-ZnO NRs decorated by SiO_2 nanospheres with the

assistance of WGM resonance which has been used to enhance the sensitivity of gas

sensors and be a cavity of lasing in many materials and circular structures.[16-19] In this

thesis, we attempt to investigate and analyze the unique properties of our optical devices.

We found that after the SiO_2 nanosphere decoration, the laser action of our devices can

be greatly improved. Morover, through varying SiO_2 nanosphere size, we found that

the laser action could be controlled by the sizs of nanosphere size.

In chapter 1, the development of random laser and the motivation of our work are

described. In chapter 2, fundamental concepts of photoluminescence (PL) and ZnO

materials are introduced. Chapter 3 presents how to prepare for our device and the

experimental setup of scanning electron microscopy (SEM), cathodoluminescence (CL),

PL, and time-resolved photoluminescence (TRPL). Chapter 4 shows the enhancement

of random laser action assisted by WGM resonance. We use the TRPL experiments,

varying the size of SiO_2 nanospheres, CL mapping, and theoretical calculation to

confirm the underlying mechanism responsible for the enhanced random laser action in

SiO$_2$ nanospheres decorated VS-ZnO NRs. The last chapter, chapter 5, decribes a brief

conclusion of this thesis.

Reference

1. V. S. Letokhov, *Sov. Phys. JETP* 1968, **26**, 835.

2. H. D. Li, S. F. Yu, S. P. Lau, and E. S. P. Leong, *Appl. Phys. Lett*. 2006, **89**, 021110.

3. M. Anni, S. Lattante, T. Stomeo, R. Cingolani, G. Gigli, G. Barbarella, and L. Favaretto, *Phys. Rev. B.* 2004, **70**, 195216

4. R. C. Polson, and Z. V. Vardeny, *Appl. Phys. Lett.* 2004, **85** 1289–1291.

5. W. Guerin, N. Mercadier, F. Michaud, D. Brivio, L. S. Froufe-Pérez, R. Carminati, V. Eremeev, A. Goetschy, S. E. Skipetrov, and R. Kaiser, *J. Opt*. 2010, **12**, 024002.

6. S. F. Yu, C. Yuen, S. P. Lau, W. I. Park, and G. C. Yi, *Appl. Phys. Lett.* 2004, **84**, 3241-3243.

7. H. Zhu, C. X. Shan, J. Y. Zhang, Z. Z. Zhang, D. X. Zhao, B. H. Li, B. Yao, D. Z. Shen, X. W. Fan, Z. K. Tang, X. H. Huo, and K. L. Choy, *Adv. Mater.* 2010, **22**, 1877-1881.

8. A. Tsukazaki, M. Kubota, A. Ohtomo, T. Onuma, K. Ohtani, H. Ohno, S. F. Chichibu, and M. Kawasaki, *Jpn. J. Appl. Phys.* 2005, **44**, L643-L645.

9. S. Chu, M. Olmedo, Z. Yang, J. Kong, and J. Liu, *Appl. Phys. Lett.* 2008, **93**, 181106.

10. C. Zhang, F. Zhang, T. Xia, N. Kumar, J. I. Hahm, J. Liu, Z. L. Wang, and J. Xu, *Opt. Express* 2009, **17**, 7893-7900.

11. M. H. Huang, *Science* 2001, *292*, 1897-1899.

12. D. J. Gargas, M. C. Moore, A. Ni, S. W. Chang, Z. Zhang, S.-L. Chuang, and P. Yang, *ACS Nano* 2010, *4*, 3270-3276.

13. R. Chen, B. Ling, X. W. Sun, and H. D. Sun, *Adv. Mater.* 2011, *23*, 2199-2204.

14. Y. T. Chen and Y. F. Chen, *Opt. Express* 2011, *19*, 8728-8734.

15. H. Cao, Y. G. Zhao, S. T. Ho, E. W. Seelig, Q. H. Wang, and R. P. H. Chang, *Phys. Rev. Lett.* 1999, *82*, 2278-2281

16. C. W. Chen and Y. F. Chen, *Appl. Phys. Lett.* 2007, *90*, 071104.

17. Y. Wu and P. T. Leung, *Phys. Rev. A* 1999, *60*, 630-633.

18. T. J. Lin, H. L. Chen, Y. F. Chen, and S. Cheng, *Appl. Phys. Lett.* 2008, *93*, 223903.

19. I. S. Grudinin, A. B. Matsko, and L. Maleki, *Phys. Rev. Lett.* 2009, *102*, 043902.

Chapter 2

Background knowledge of experimental technique and studied nanomaterials

2.1 Theory of photoluminescence of semiconductors

Photoluminescence (PL) is a non-destructive optical technique used for the characterization, investigation, and detection of point defects or for measuring the band-gaps of materials. Photoluminescence involves the irradiation of the crystal to be characterized with photons of energy greater than the band-gap energy of that material. In the case of a crystal scintillator, the incident photons will create electron-hole pairs. When these electrons and holes recombine, this recombination energy will transform partly into non-radiative emission and partly into radiative emission.

As shown in Fig 2.1, we can briefly say photoluminescence process includes three main phases: [1](1) Excitation: Electrons can absorb energy from external sources, such as lasers, arc-discharge lamps, and tungsten-halogen bulbs, and be promoted to higher energy levels. In this process electron-hole pairs are created. (2) Thermalization: Excited pairs relax towards quasi-thermal equilibrium distributions. (3) Recombination: The energy can subsequently be released, in the form of a lower energy photon, when

the electron falls back to the original ground state. This process can occur radiatively or

non-radiatively.
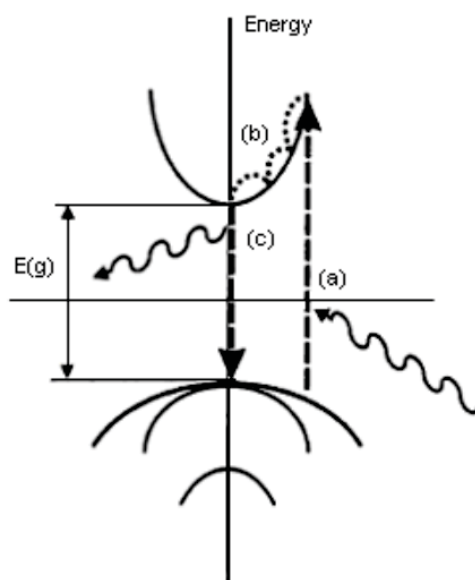
Fig. 2.1　The schematic of photoluminescence. (a) An

electron absorbs a photon and is promoted from the

valence band to the conduction band. (b) The electrons

cool down to the bottom of the conduction band. (c) The

electron recombines with the hole resulting in the

emission of light with energy hv.

　　When a semiconductor absorbs a photon of energy greater than the band gap, an

electron is excited from the valence band into the conduction band leaving behind a hole.

When the electron returns to its original state, its energy may be released through

radiative (release of a photon) or non-radiative (no photon production) recombination.

When the electron and hole recombine through radiative recombination, a photon is

emitted and the energy of the emitted photon is dependent on the change in energy state

9

of the electron-crystal system.

A simplified set of radiative transitions that lead to emission in semiconductors is

giving in Fig. 2.2.
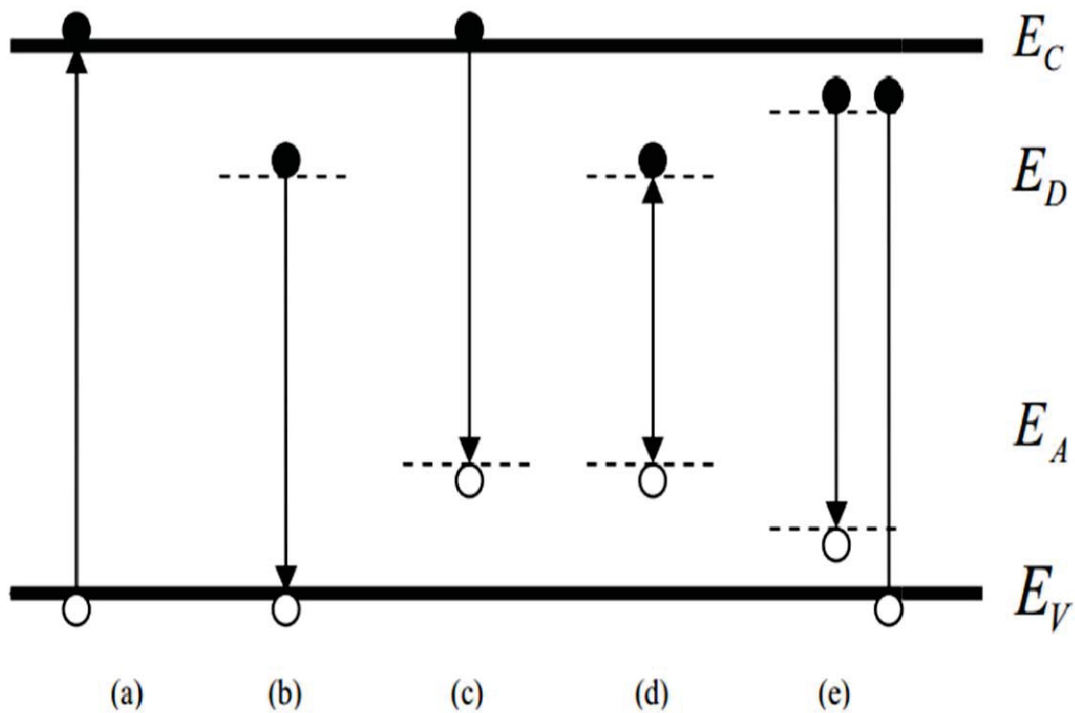
Fig. 2.2 Schematic diagram of common radiative transitions observable with photoluminescence transitions.

Process (a) : Process (a) is the band to band transition, which dominates at room

temperature and can be used to estimate the material bandgap energy (Eg). For indirect

semiconductors, a band-to band recombination process is unlike because the electrons at

the bottom of the conduction band have a nonzero crystal momentum with respect to the
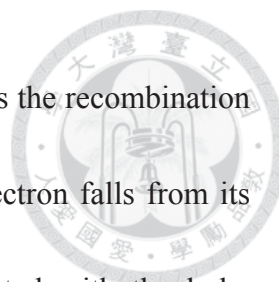
holes at the top of the valence band. Band to band transition contains the recombination

of free electrons and free holes. This transition occurs when an electron falls from its

conduction band state into the empty valence band state associated with the hole.

Band-to-band transition depends on the density of available electrons and holes, and the

probability is proportional to the absorption coefficient. The photon energy, which is

equal to the energy difference between the excited and ground states, released during

the process usually produces a photon and emits light in a semiconductor having a

direct band gap. It is given by the equation:
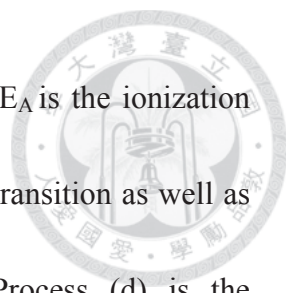
$$h\nu = E_f - E_i \qquad\qquad (2.1)$$

where E_f and E_i are, respectively, the final and initial state energies. In indirect

semiconductors, band-to-band recombination occurs with phonon contribution and

emitted photon energy is

$$h\nu = E_f - E_i \pm h\Omega \qquad\qquad (2.2)$$

Where $h\Omega$ is the energy of phonon.(as shown in Fig2.3)

Process (b), (c), (d): At temperature for which k_BT is greater than the ionization

energy of shallow impurities, these impurities are ionized, hence band-to-band transition

dominate. At sufficiently low temperature the thermal energy of carriers becomes

smaller than the ionization energy of the impurities in which case are frozen to the

impurity. For example, in a p-type material containing N_A acceptors per unit volume,

holes are trapped at the acceptor if k_BT is smaller than E_A, where E_A is the ionization

energy of the acceptor. Process b represents the donor-to-free-hole transition as well as

process (c) represents the free-electron-to-acceptor transition. Process (d) is the

donor-acceptor pair (DAP) recombination. Donor is substitutional atom with a higher

number of valence electrons compared with the host atom, where as acceptor is a

substitutional atom with lower of valence electrons. Donor contributes excess electrons

to the crystal, while acceptor tends to capture electrons or equivalently donate holes.

Donor or acceptor may be electrically charged or neutral.[2] As the neutral donor and the

neutral acceptor are brought closer together, the donor's electron become increasingly

shared by the acceptor. In other words, the donor and the acceptor become increasingly

more ionized and form a pair.[3] The energy of the DAP recombination emission in

relatively pure crystals can be expressed by:

$$h\nu(r) = E_g - (E_A - E_D) + e^2/\varepsilon r \qquad (2.3)$$

where E_A and E_D are the binding energies of the acceptor and donor, respectively, ε is

the dielectric constant, e is the electron charge, and r is the distance between the donor

and acceptor impurities which participate in the recombination. The last term arises

from the coulombic interaction of the carriers and depends on the separation r. the

radiative transition probability in this case is

$$P(r) = P(0)\exp(-2r/a) \qquad (2.4)$$
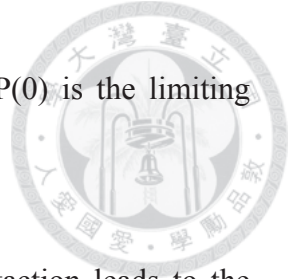
where a is the Bohr radius of the less tightly bound center, and P(0) is the limiting transition probability which is a constant as r~0.
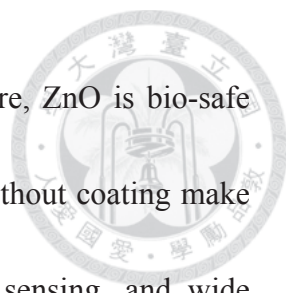
Process (e): Process (e) is exciton transition. Coulombing attaction leads to the formation of an excited state in which an electron and the hole remain bound to each other in a hydrogen-like state, referred as a free exciton.[4] The energy of the emitted photon is

$$h\nu = E_g - E_X \tag{2.5}$$

where E_g is the bandgap energy of the semiconductor and E_X is the Coulomb energy of the exciton. In reality, many semiconductor materials contain small amounts of natural defects or impurities forming neutral donors and acceptors. Optically generated free excitons can interact with those impurities and may become captured by them. They are then called donor-bound or acceptor-bound excitons depending on whether the impurity that the exciton attached is a donor or an acceptor.

2.2 ZnO nanorods
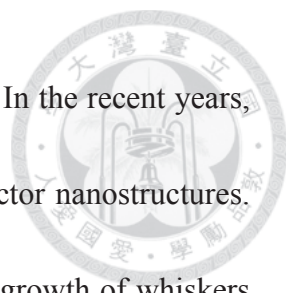
In the past decade global research interest in wide band gap semiconductors has been attracted towards zinc oxide (ZnO) due to its excellent properties as a semiconductor material. Zinc oxide (ZnO) is a direct band-gap (E_g = 3.37 eV) semiconductor with a large exciton binding energy (60 meV), exhibiting near UV

13

emission, transparent conductivity and piezoelectricity.[5] Furthermore, ZnO is bio-safe

and biocompatible, and may be used for biomedical applications without coating make

ZnO suitable for optoelectronics, transparent electronics, lasing, sensing, and wide

range of applications.[5-8]

Other basic characteristics of ZnO are the polar surfaces that are formed by

charged ions produced by positively charged Zn^+ (0001) and negatively charged O^-(000

$\bar{1}$) polar surfaces. It is responsible for the spontaneous polarization observed in ZnO.

The polar surfaces of ZnO have non-transferable and non-flowable ionic charges. The

interaction among the polar charges at the surface depends on their distribution.

Therefore the structure is arranged in such a way to minimize the electrostatic energy,

which is the main driving force for growing polar surface dominated nanostructures.

This effect results in a growth of various ZnO nanostructures such as nanorods,

nanosprings, nanocages, nanobelts, nanocombs, nanorings, and nanohelices.[5]

Additionally, in recent years, one-dimensional (1D) nanostructures such as rods,

wires, belts have attracted much attention due to their many unique properties and the

possibility that they may be expected to play an important role as both interconnects and

functional units in fabricating electronic, optoelectronic, electrochemical and

electromechanical nanodevices. It is generally accepted that 1D nanostructures are

useful materials for investigating the dependence of electrical and thermal transport or

mechanical properties on dimensionality and quantum confinement. In the recent years, much effort has been devoted to developing various 1D semiconductor nanostructures. Vapour–liquid–solid (VLS) and vapour–solid (VS) mechanisms for growth of whiskers or fibres at high temperature are well recognized, and have been used to synthesize various group III–V and II–VI compound semiconductor nanostructures. Intensive research has been focused on fabricating 1D ZnO nanostructures and in correlating their morphologies with their size-related optical and electrical properties. Many different kinds of ZnO nanostructures have been developed, such as nanodots, nanorods, nanowires, nanobelts, nanotubes, nanobridges and nanonails, nanowalls, nanohelixes, and nanorings. Among these various types of nanostructure, ZnO nanorods and nanowires have been the most widely studied because of their easy formation and device applications.[2, 9-10]

Reference

1. Y. Yu, M. Cardona, *Fundamentals of Semiconductors*, pp.348, published by springer, 1990.

2. Quirk, M.; Serda, *J. Semiconductor Manufacturing Technology*, Prentice Hall, 2000.

3. Xu, Y.; Sheng, K.; Li, C.; Shi, G. ACS Nano 2010, 4, 4324-4330.

4. H. K. Schröeder, *Semiconductor Material and Device Characterization*, published by John Willey & Sons, 1998, 624,

5. Chen Z.; Ren, W.; Gao, L.; Liu, B.; Pei, S., Cheng, H. M. Nat. Mater. 2011, **10**, 424-428.

6. O. Dulub, L. A. Boatner, and U. Diebold, Surf. Sci. **519**, 201 (2002)

7. Z. L. Wang, J. Phy. Condens. Matter **16**, 829 (2004)

8. T. Kogure, and Y. Bando, J. Electron Microsc. **47**, 7903 (1993)

9. Park, S. Ruoff, R. S. Nature Nanotech. 2009, **4**, 217-224.

10. Seung J. C.; Fethullah G.; Ki K. K.; Eun S. K.; Gang H. H.; Soo M. K.; Hyeon J. S., Seon M. Y.; Jae Y. C.; Min H. P.; Cheol W. Y.; Didier P.; Young H. L.; Adv. Mater. 2009, 21, 2328-2333.

Chapter 3

Experimental details, Theoretical background and Sample preparation

3.1 Scanning Electron Microscopy (SEM)
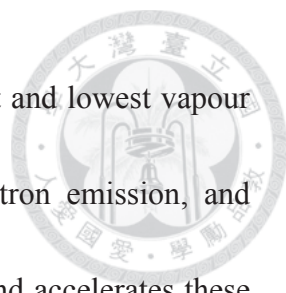
The scanning electron microscope (SEM) is a type of electron microscope that images the sample surface by scanning it with a high-energy beam of electrons in a raster scan pattern.[1-2] With irradiating the sample with electron beam in a vaccum chamber, secondary electrons (SE), backscattered electrons (BSE), characteristic x-rays and other signals are generated as indicated in Fig 3.1.[3] The SEM mainly utilizes SE or BSE signals to form an image. SE are produced near the sample surface, and SE image obtained upon detecting these electrons reflects the fine topographical structure of the sample. BSE are beam electrons that are reflected from the sample by elastic scattering. BSE are often used in analytical SEM along with the spectra made from the characteristic X-rays, and BSM image therefore reflects the compositional distribution on the sample surface. Because the intensity of the BSE signal is strongly related to the atomic number (Z) of the specimen, BSE images can provide information about the distribution of different elements in the sample. Moreover, x-ray detector can be equipped to the SEM, so the SEM is also applicable as an x-ray analyzer for

determining what elements are included in the sample.
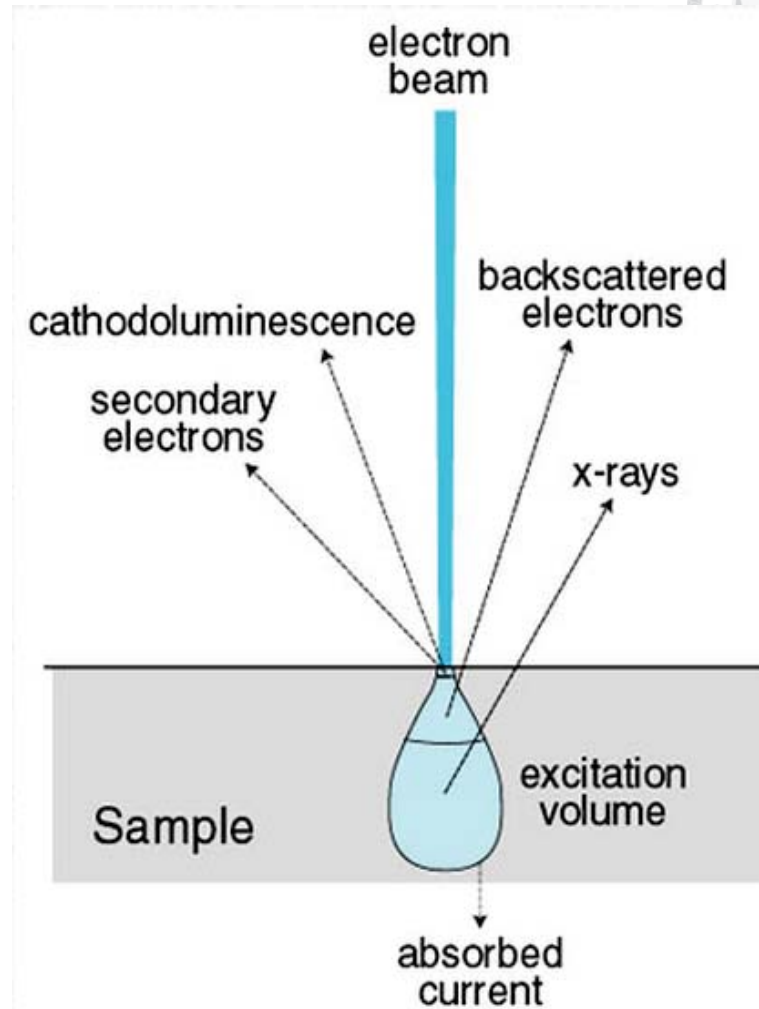
Fig. 3.1 Signals that result from electron beam-specimen interaction.

The typical SEM instrument is made up of electron column, scanning system, detector(s), display, vacuum system and electronics controls as shown in Fig. 3.2. [4] The electron column of the SEM consists of an electron gun and two or more electromagnetic lenses operating in vacuum. An electron beam is thermionically emitted from an electron gun fitted with a tungsten filament cathode. Tungsten is normally used

in thermionic electron guns because it has the highest melting point and lowest vapour pressure of all metals, thereby allowing it to be heated for electron emission, and because of its low cost. The electron gun generates free electrons and accelerates these electrons to energiesin the range 1-40 keV in the SEM. With the the electromagnetic lenses (condenser and objective lenses), the electron beam generated by the electron gun is coveraged into a fine beam in a high-vacuum column. Typically the electron beam is defined by probe diameter, probe current and probe convergence. And by applying a scan signal to the deflection coils, the electron beam is scanned along the sample surface in X and Y direction. Objective lens is used to converge the electron beam into a fine beam and focus it onto the sample surface. When the primary electron beam interacts with the sample, the electrons lose energy by repeated random scattering and absorption within a teardrop-shaped volume of the specimen known as the interaction volume, which extends from less than 100 nm to around 5 μm into the surface. The energy exchange between the electron beam and the sample results in the reflection of high-energy electrons by elastic scattering, emission of secondary electrons by inelastic scattering and the emission of electromagnetic radiation, each of which can be detected by specialized detectors. A secondary electron detector for detecting signals produced from the sample could converts signal to electric one. Finally the photomultiplier are used to amplify the signals, the amplified electrical signal output is displayed as a

two-dimensional intensity distribution that can be viewed and photographed on a video

display, which are displayed as variations in brightness.
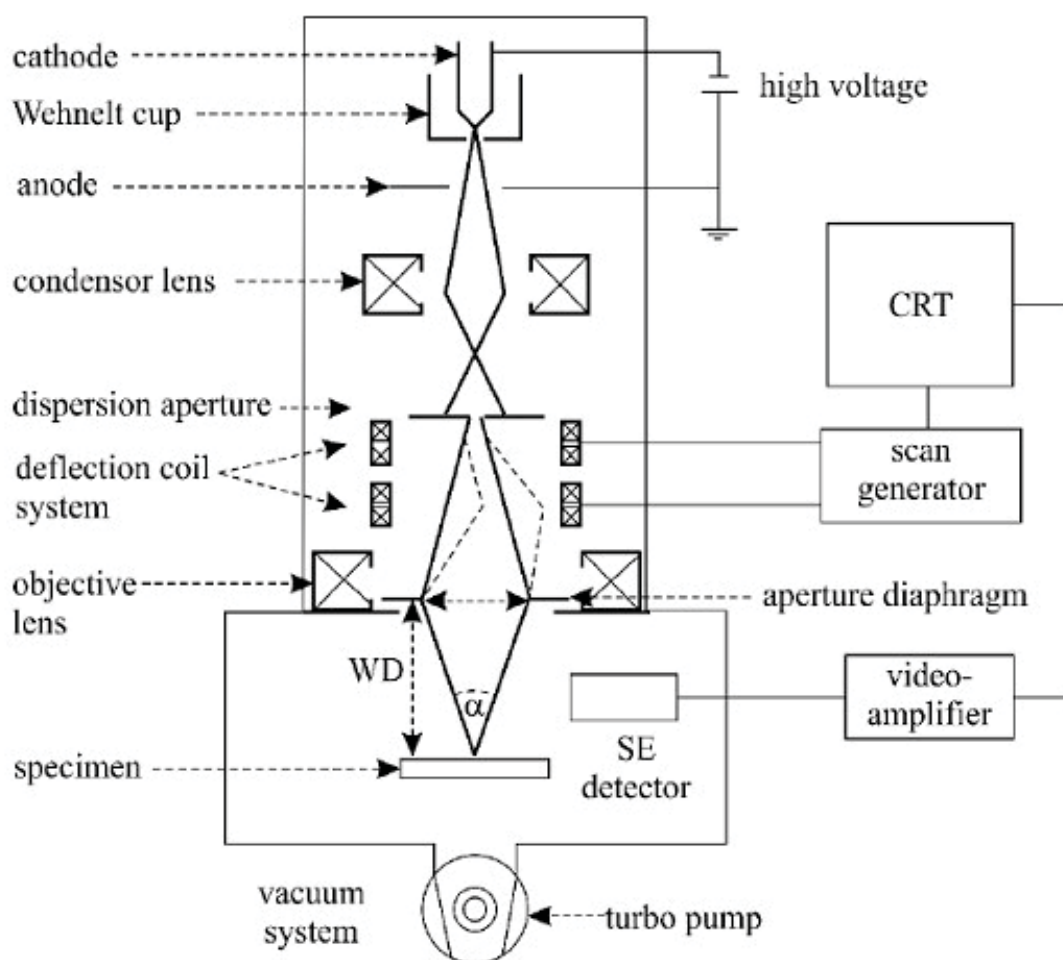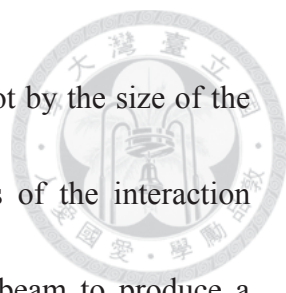
Fig. 3.2 The structural scheme of a typical scanning electron microscope.

When imaging in the SEM, samples must be electrically conductive at the surface,

and electrically grounded to prevent the accumulation of electrostatic charge at the

surface. Metal objects require cleaning and mounting on a specimen stub for SEM. It

tend to charge when scanned by the electron beam for nonconductive specimens, and

this causes scanning faults and other image artifacts especially in secondary electron

imaging mode. Therefore, they are usually coated with an ultrathin coating of

electrically conducting material by sputter coating or evaporation. Additionally, coating

could increase signal/noise ratio for samples which is composed of low atomic number

(Z) atoms. This improvement arises because secondary electron emission for high-Z

materials is enhanced. Figure 3.3 show a photo of the SEM (JEOL, JSM-6500F) image

used in this work.

Fig. 3.3 Photo of scanning electron microscopy
(JSM-6500F, JEOL)

The image details and resolution in the SEM are determined not by the size of the electron probe by itself but rather by the size and characteristics of the interaction volume, which is the area of the sample excited by the electron beam to produce a signal. When the accelerated beam electrons strike a specimen they penetrate inside it to depths of about 1 μm and interact both elastically and inelastically with the solid, forming a limiting interaction volume from which various types of radiation emerge, including BSE, SE, characteristic and brehmsstrahlung x-rays, and cathodoluminescence in some materials. The combined effect of elastic and inelastic scattering controls the penetration of the electron beam into the solid. The resulting region over which the incident electrons interact with the sample is known as interaction volume. The interaction volume has several important characteristics, which determine the nature of imaging in the SEM. The energy deposition rate varies rapidly throughout the interaction volume, being greatest near the beam impact point. The interaction volume has a distinct shape as shown in Fig 3.4. For low-Z target it has distinct pear shape. For intermediate and high-Z number materials the shape is in the form of hemi-sphere. The interaction volume increases with increasing incident beam energy and decreases with increasing average atomic number of the specimen. For secondary electrons the sampling depth is from 5 to 50 nm and diameter equals the diameter of the area emitting backscattered electrons. BSE are emitted from much larger depths

compared to SE. Finally the resolution in the SEM is controlled by the size of the

interaction volume.

The effective interaction volume can be calculated using the electron range (R): [5]

$$R = \frac{0.0276 A E_0^{1.67}}{\rho Z^{0.89}} \, (\mu m)$$

Where A is the atomic weight (in g/mole), Z is the atomic number, ρ is the density

(in g/cm^3), and E$_0$ is the energy of electron beam (in KeV)
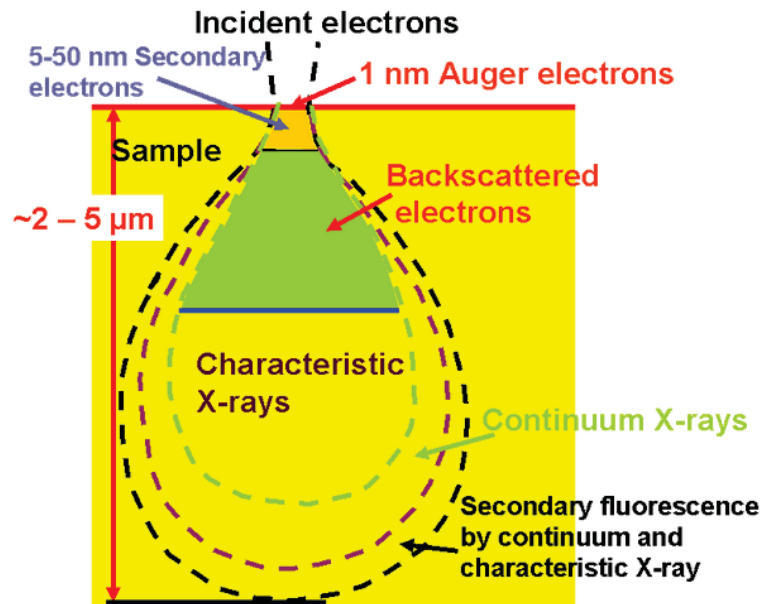
Fig. 3.4 The range and spatial resolution of backscattered

electrons, secondary electrons, X-rays, and Auger

electrons for electrons incident on a solid.

23

3.2 Cathodoluminescence (CL)

When an electron is promoted into the conduction band, the electron and hole become free and they can move independently in corresponding bands.[6] The major electron-hole recombination pathway between the conduction and valence bands involve donor and/or acceptor levels, recombination via deep level traps, and recombination at the surface. Electron beam excitation in general leads to emission by all the luminescence mechanisms present in the material. Photoluminescence emission may strongly depend on the excitation hv, which can be used for selective excitation of particular emission processes. Cathodoluminescence analysis of materials, on the other hand, can provide depth-resolved information by varying the electron beam energy as shown in Fig 3.4. In general, electron beam energy of upon to 30 keV can be used. Cathodolumiscence analysis enables one to assess various properties of the material with a spatial resolution down to 1 μm or less. Spectroscopic CL and monochromatic imaging can be used in identification and measurement of luminescence center concentration and distributions, as well as in the determination of the composition of compound materials.

Here, the CL spectrometer (Gatan, MonoCL3) as shown in Figs. 3.5 is adapted to the SEM with the energy of electron beam from 1kVto 30 kV.   PMT and detectors are used to gathered the visible and IR emission spectra.

Fig. 3.5 Photo of the CL spectrometer.

3.4 Photoluminescence (PL) arrangement

Fig 3.6 illustrates the photoluminescence setup. In this research work, PL measurements

were performed at room temperature by using laser lines with a wavelength of 266 nm from a

pulsed laser as an excitation source. The PL measurement has three main steps, in the first step,

the semiconductor is optically excited to create electron-hole pairs. Different kinds of lasers

such as He-Cd laser and Ar+ laser with wave lengths of 266 nm are used for the excitations in
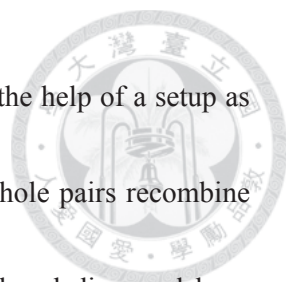
ZnO. The laser beam is then projected on the semiconductor sample with the help of a setup as shown in the schematic diagram. In the second step, the excited electron-hole pairs recombine radiatively and emit light. In the final step, the emitted light is detected and dispersed by a double grating monochromator and photomultiplier detectors. The final spectrum is collected and analyzed in a computer.

The intensity of the PL signal apparently depends on the material's quality, the system throughout, and detector sensitivity. The resolution of the system, its ability to accurately measure energy, is determined by the focal length of the monochromator, where the grating spacing sets the wavelength coverage. At long wavelength a PMT with a GaAs or other composite cathode is useful. Gemanium photodiodes are good for the near-infrared range.
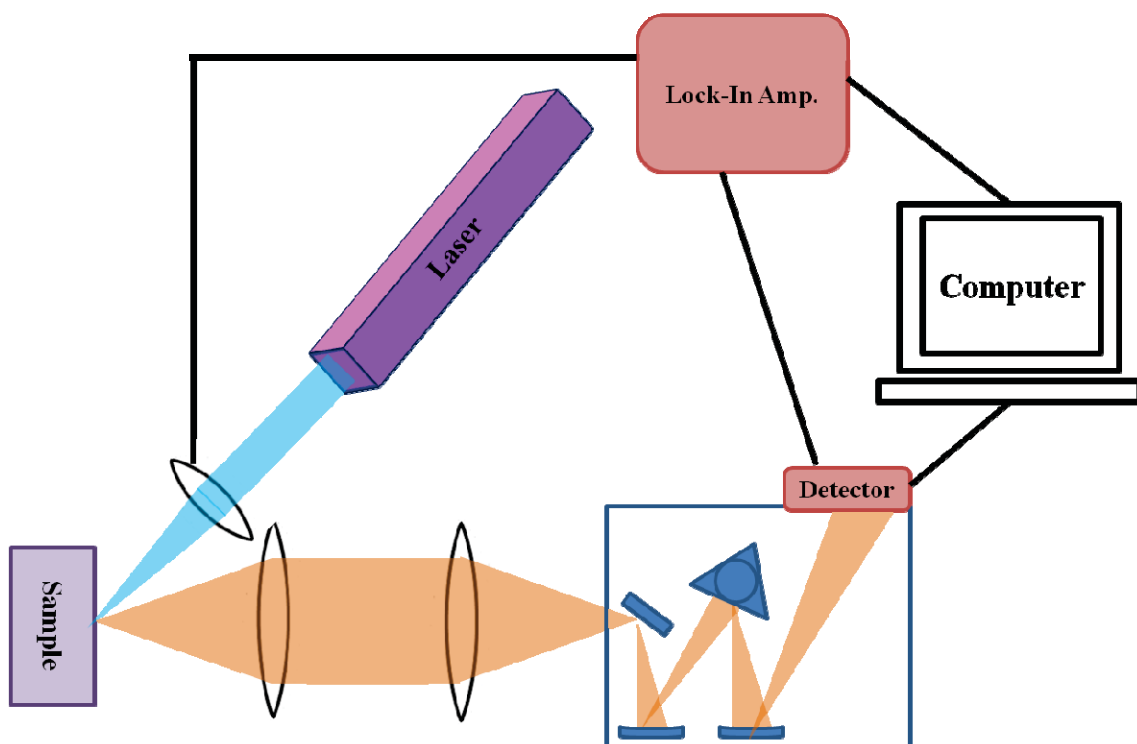
Figure 3.6: The photoluminescence experiment setup.

3.5 Time-resolved photoluminescence

Time resolved photoluminescence (TRPL) is used to investigate the carrier dynamics which is a sensitive and powerful technique to record the transient PL decay curve. Unlike the steady-state PL measurement, time-resolved data frequently contain more information than is available from the steady-state data. In a TRPL measurement the sample is excited with a very short and intense light pulse, and the luminescence is measured with the necessary temporal resolution. Luminescence intensities of the transitions depend on the corresponding recombination rates. Because the recombination rate depends on the carrier populations in the participating states, the carrier populations in different states can be calculated as a function of time. Therefore, also the transition processes between the participating states can be studied. Immediately after the excitation pulse even more rapid processes have a major role, but due to the limitations of the detection system and the rate-equation model these processes were not studied in this thesis.

Figure 3.7 shows schematically the TRPL measurement system used in this work. The basic optics, beam focusing, sample cooling, luminescence collimating and monochromator were the same as in the continuous wave PL (CWPL) measurement system. The excitation pulse source was a mode locked titanium sapphire laser operating at the wavelength of 266 nm. The photon counting system uses a

multichannel plate photomultiplier as a detector. Excitation laser pulses are detected by

a silicon photodiode. The system measures the time between the detected PL photon

and the next laser pulse. The system assumes, that only one photon is detected between

two pulses. The temporal resolution of the photon counting system is about 30 ps. It is

mainly determined by the photo multiplier tube.
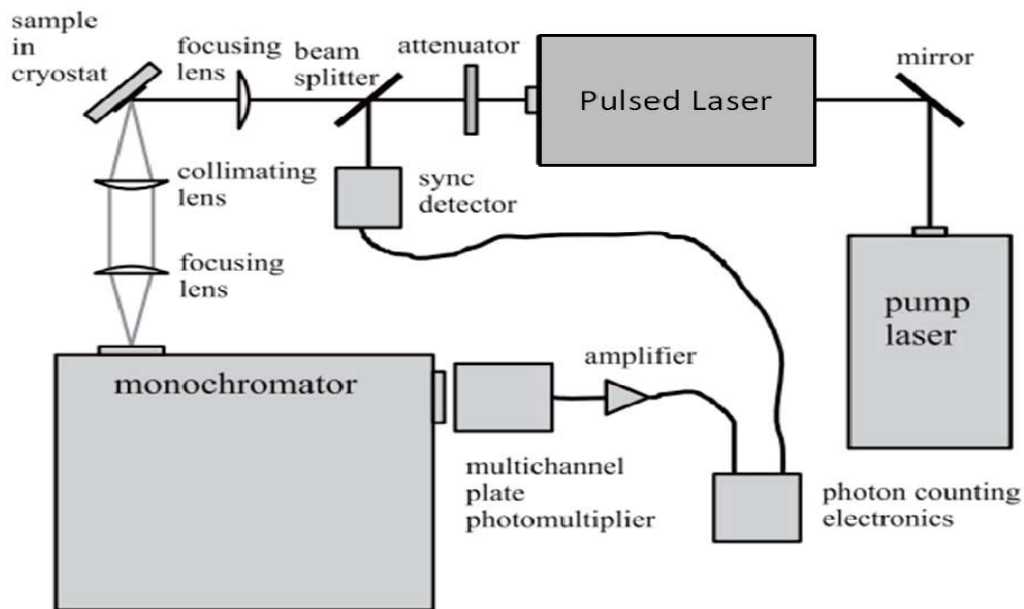
Figure 3.7: The time-resolved PL setup

3.6 Absorption Spectroscopy

Absorption spectroscopy is a optical technique that measures the absorbance of the

incident light, as a function of wavelength, due to the interaction between the

electromagnetic field and the sample. Absorption spectroscopy is employed as an

analytical tool to determine the band gap of semiconductor, energy level of the excited

states of nanoparticles, resonant frequency of surface plasmon of noble metals and etc.

In general, the infrared and ultraviolet-visible spectroscopy is used in academic

researches. There are many approaches to measuring absorption spectra. The most

common arrangement is to focus a beam of light on a sample and detect the intensity of

the incident light that passes through it. As shown in Fig. 3.8, a Xe lamp and Spectra

Pro 300i monochromator were used as a tunable wavelength of incident light source.

The white light emitted from the Xe lamp can be separated different single wavelength

of incident light source by the monochromator. In order to detect a specific transmission

signal, the signal was recorded by a Si/Ge detector.
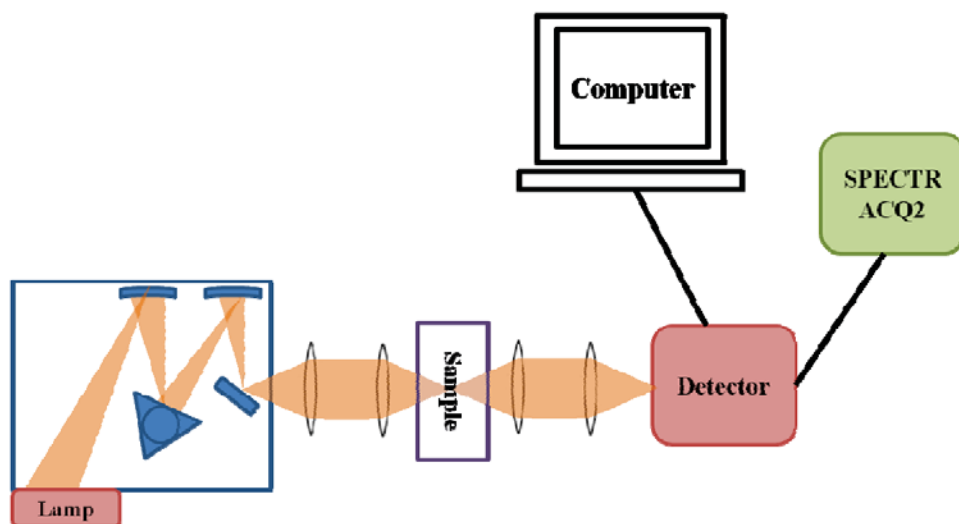
Figure 3.8: The absorption spectroscopy setup.

3.7 Vapor-Soild (VS) Growth Mechanism of ZnO Nanorods

The VS process grows to form wirelike or beltlike nanostructure with the oxide vapor higher temperature region. It cannot be explained that how atoms and building blocks can be rationally assembled into one-dimension wirelike or beltlike nanostructure. The studied ZnO NRs in this work were fabricated by the VS growth mechanism.[7] A sapphire substrate was placed on the top of alumina boat loaded with a high purity Zn powder (99.99%), and the whole alumina boat was located at the center of a tube furnace. Subsequently, the reaction chamber was evacuated and kept at a pressure of 10 Torr when argon and oxygen with a high purity of 99.9% were introduced into the reaction chamber at a flow rate of 200 sccm and 5 sccm, respectively. In addition, the growth temperature was maintained at 620°C and the dwell time was one hour. After the fabrication, VS-ZnO NRs were formed uniformly over the entire substrate.

References

1. Online resource, http://en.wikipedia.org/wiki/Scanning_electron_microscope.

2. D. McMullan, *Scanning*, 2006, **17**, 175.

3. Online source, http://www4.nau.edu/microanalysis/Microprobe-SEM/Signals.html

4. S. Fatikow, *"Nanostructuring and Nanobonding by EBID"*. Automated nanohandling by Microrobts, 2007, Chapter 1.

5. K. Kanaya, S. Okayama, *J. Appl. Phys.* 1972, **5**, 43

6. B. G. Yacobi and D. B. Holt, *Cathodoluminescence microscopy of inorganic solids*, Plenum Press, New York and London (1990)

7. A. Umar, S. H. Kim, Y. S. Lee, K. S. Nahm, and Y. B. Hahn, *J. Cryst. Growth* , 2005, *282*, 131-136.

Chapter 4
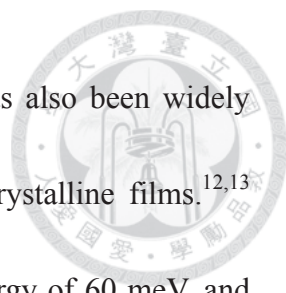
Enhancement of Random Laser Action Assisted by

Whispering-Gallery-Mode Resonance

4.1 Introduction

In recent years, random lasing is a phenomenon that has been extensively investigated in some disordered media for its unique properties and potential applications, since the original idea proposed by Letokhov.[1-5] Comparing with the conventional laser action due to Fabry-Perot resonance, random lasing necessitates no mirror cavities to achieve coherent feedback in the laser system with its low-cost and simple process technology. Moreover, random lasing usually exhibits a very broad angular distribution which is ideal for display application. In random lasers, cavities are self-formed, and coherent feedback is provided by scattering events in the random medium. As the close-loop is formed in the cavities and the gain exceeds the loss, random laser action can be achieved. A high gain medium and efficient light scattering centers are therefore required for the accomplishment of random lasing.

Recently many nanoscale optoelectronic devices have been extensively developed because of their low dimensionality and quantum confinement effect, such as

transistors,[6,7] photodetectors,[8,9] and emitters.[10,11] Random lasing has also been widely studied in nanoscale materials such as nanorod arrays and nanocrystalline films.[12,13] ZnO, with a wide bandgap of 3.37 eV , a high exciton binding energy of 60 meV, and plenty kinds of nanostructures, is very suitable for the fabrication of ultraviolet light-emitting diodes and laser devices with high efficiency.[14-16] In addition, due to a high refractive index in ultraviolet region (~ 2.5), the total internal reflection in ZnO structures can be easily achieved. Based on these favorable properties, conventional laser actions from ZnO nanostructures have been successfully demonstrated by Fabry-Perot cavities, whispering-gallery-mode (WGM) cavities and different types of resonators.[17-19] However, according to previous studies,[20] the emission of ZnO nanorods (NRs) fabricated by vapor-solid (VS) growth mechanism exhibits a very broad spectrum and the quantum efficiency of random laser action is rather poor.[5,13]

Here, we provide an alternative approach to enhance the random lasing behavior arising from VS-ZnO NRs decorated by SiO_2 nanospheres with the assistance of WGM resonance. WGM resonance has been used to enhance the sensitivity of gas sensors, such as the detection of CO_2 and H_2O, and WGM lasing has also been demonstrated in many materials and circular structures.[21-24] In this study, it is found that after the nanosphere decoration, the differential quantum efficiency can be greatly enhanced and the emission spectra show only very sharp peaks with a full width at half maximum

(FWHM) less than 0.3 nm and a very narrow background signal. Time-resolved

photoluminescence (TRPL) experiments have also been performed to verify the induced

laser action. Through varying SiO_2 nanosphere size, cathodoluminescence (CL)

mapping and theoretical calculation, we firmly confirm that WGM is indeed the

underlying mechanism responsible for the enhanced random laser action in SiO_2

nanospheres decorated VS-ZnO NRs. Our result shown here should be very useful for

the future development of highly efficient light emitting devices.
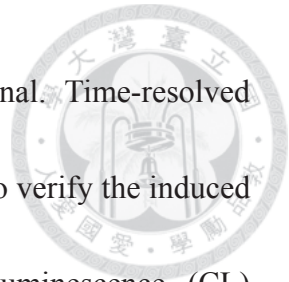
4.2 Experiment

The studied ZnO NRs in this work were fabricated by the VS growth mechanism.[25] A sapphire substrate was placed on the top of alumina boat loaded with a high purity Zn powder (99.99%), and the whole alumina boat was located at the center of a tube furnace. Subsequently, the reaction chamber was evacuated and kept at a pressure of 10 Torr when argon and oxygen with a high purity of 99.9% were introduced into the reaction chamber at a flow rate of 200 sccm and 5 sccm, respectively. In addition, the growth temperature was maintained at 620°C and the dwell time was one hour. After the fabrication, VS-ZnO NRs were formed uniformly over the entire substrate.

To investigate random laser action, the samples were optically excited by a Q-switched Nd: yttrium aluminum garnet laser (266 nm, 3–5 ns pulse, 10 Hz) focused to a beam size about 200 μm in diameter. TRPL experiment was performed at room temperature excited by a 260 nm pulse laser. The cathodoluminescence (CL) mapping images were carried out on the same SEM instrument equipped with Gatan-Mono-CL3 operating at 10 kV. All measurements were performed at room temperature.
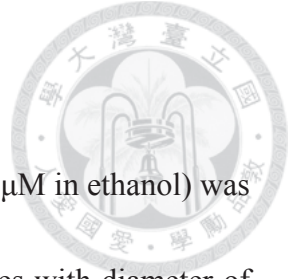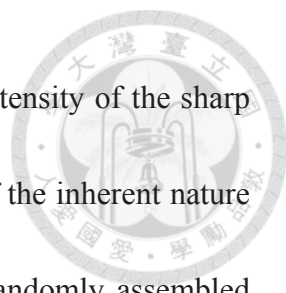
4.3 Results and Discussion

For the studied devices, a droplet of 2 μL SiO$_2$ nanospheres (10 μM in ethanol) was deposited on VS-ZnO NRs. Three different sizes of SiO$_2$ nanospheres with diameter of 120 nm, 190 nm, and 250 nm were used. The morphology of the composite consisting of VS-ZnO NRs and SiO$_2$ nanospheres was characterized by scanning electron microscopy (SEM) (JSM 6500, JEOL). It is clearly seen in **Figure 4.1** that VS-ZnO NRs have lengths about 5 ~ 8 μm and diameters ranging between 100 nm and 500 nm. As shown in Figure 4.1a, the SiO$_2$ nanospheres with a diameter about 120 nm are randomly deposited on VS-ZnO NRs.
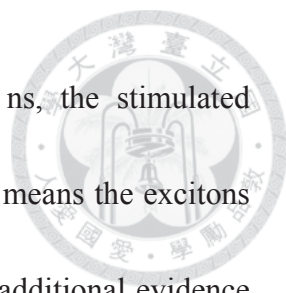
The emission spectra of pristine VS-ZnO NRs under different pumping energy illuminated with 266 nm pulsed laser are shown in **Figure 4.2**a. We only observe a very broad spontaneous emission spectrum at around 389 nm with a FWHM of about 12 nm which is similar to previous report.[20] As the pumping energy increases, the emission intensity increases gradually without any indication of sharp peaks which can be used to identify as the occurrence of laser action.

The emission spectrum of SiO$_2$ nanospheres decorated VS-ZnO NRs is shown in Figure 4.2b. Quite interestingly, after decorating nanospheres, the FWHM of whole emission spectrum is reduced to 1.9 nm and the light intensity is greatly enhanced. As the pumping energy increases, several sharp laser-like emission peaks superposed on the

broad spontaneous emission. We also found that the position and intensity of the sharp

peaks randomly change at different moment, which is a signature of the inherent nature

of random lasing behavior.[5,12] The emission characteristic of the randomly assembled

VS-ZnO NRs as shown in Figure 2b can therefore be attributed to random laser action,

which is achieved when specific frequencies of light are multiply amplified by

stimulated emission in randomly closed loop paths.

To further examine the laser action, **Figure 4.3**a shows the analysis of the

dependence of the emission intensity on pumping energy. We can clearly see that there

is an abrupt change of the slope, which provides a signature for the occurence of

stimulated emission. The value of the lasing threshold is approximately 52 μJ, impling

that the laser action can be easily achieved compared with previous reports.[20] The

differential quantum efficiency (η_d) defined as photons emitted per radiative

electron-hole pair recombination above threshold, can be determined by $\eta_d = P_O/P_I$,[26]

where P_O and P_I are the output and input pumping power, respectively. It is found that

the differential quantum efficiency (η_d) of ZnO NRs decorated with 120 nm SiO_2

nanospheres is about 7.3 times larger than the efficiency without 120 nm SiO_2

nanospheres as shown in Figure 3a. Moreover, TRPL experiments of the spontaneous

emission (by pristine ZnO nanorods) and stimulated emission (by SiO_2/ZnO composite)

monitored at 389 nm are shown in Figure 4.3b. While the spontaneous emission exhibits

a biexponential decay with time constants of 798 ps and 2.56 ns, the stimulated

emission shows shorter decay times with 516 ps and 2.09 ns which means the excitons

recombine with higher recombination rate.. This result provides an additional evidence

to support the laser action in SiO_2 nanospheres decorated ZnO NRs according to

previous reports.[2,27]

Let us now try to understand the hidden mechanisms for the induced laser action

and high differential quantum efficiency as observed above. There are two main

possible mechanisms for the improved lasing characteristics arising from the decoration

of SiO_2 nanospheres. First, there is a large contrast in refractive index between SiO_2

nanospheres and air, and the surface of ZnO NRs becomes rougher after the SiO_2

nanosphere deposition. The emitted light beam can thus be strongly scattered by SiO_2

nanospheres, which makes light travel more randomly. Therefore, random laser action is

more easily achieved, and the threshold pumping energy is reduced. Second, due to the

total internal reflections of light at the circular boundary, the spherical-shaped dielectric

cavity could support WGM resonance. Once ZnO NRs is pumped by laser, the emissive

light will prefer to incident in SiO_2 nanospheres than air because the refractive index of

SiO_2 is nearer to it of ZnO NRs. After resonating in the SiO_2 nanospheres, the intensity

of light with the specific frequency will be greatly enhanced with the reduced width of

emission spectrum, and it will induce more stimulated emission when the enhanced

light propagates with a closed-loop path among ZnO NRs with higher recombination rate. Consequently, the emission spectrum is much narrower and the random laser action is achieved. **Figure 4.4** illustrates the underpinned mechanisms responsible for the enhanced laser action assisted by the decoration of SiO_2 nanospheres.

To explore the possibility that WGM resonance is indeed responsible for the enhanced laser action, firstly we examine the Q factor which is an important parameter to describe laser cavity. From the experimental data, the Q factor is estimated to be 760 by the definition $Q = \lambda/\Delta\lambda$, where λ is the peak wavelength and $\Delta\lambda$ is the line-width of the peak. Considering the WGM in a spherical cavity, the Q factor can be determined by the following equation: [28]

$$Q = \frac{\sqrt{3}\pi D m n R^{m/4}}{2\lambda(1-R^{m/2})} \sin\left(\frac{2\pi}{m}\right),$$

(1)

where D is the diameter of SiO_2 nanospheres, m is an integer, R is the reflectivity of the boundary, n is the refractive index. If the experimentally obtained Q factor and m=6 (for WGM) is inserted into the equation, it can be deduced that the reflectivity is about 99.6% for a WGM cavity, which is reasonable for the total internal reflection on the boundary of SiO_2 nanospheres.

Secondly, we theoretically calculate the resonant WGMs due to nanoscale SiO_2

spherical cavity. [29] The main idea is that a light wave interferes with itself when having

completed one full circulation within the resonator of SiO_2 nanospheres. In order to

generate the constructive interference, the total phase shift of the wave along its path

has to be an integer multiple of 2π. Taking into account of the polarization-dependent

negative phase shift that occurs during the process of total internal reflection, we obtain

the following equation by considering the condition of spherical cavity: [23]

$$R_i = \frac{\lambda}{m_2 \pi}\left[N + \frac{2}{\theta_i}\tan^{-1}\left(\beta\sqrt{m_2^2\tan^2\theta_i - m_1^2\csc^2\theta_i}\right)\right].$$

(2)

The factors m_1 and m_2 are the reflective indices of air and SiO_2 nanospheres

respectively. β depends on the polarization of light wave, i.e., for the TM polarization

$\beta_{TM} = m_2^{-1}$ and for the TE polarization $\beta_{TE} = m_2$. R_i is the geometric parameter, which is

the diameter of SiO_2 nanospheres. θ_i is the angle of the incidence of the circulating light.

According to the theoretical calculation, the WGM for the TE polarization does not

exist, which is consistent with the previous investigation of laser action in cylindrical

cavity.[23] For 120 nm SiO_2 nanospheres, the TM-resonance peak position obtained by the

theoretical calculation is approximately at 389 nm for N=1. It is in good agreement with

the emission peak of SiO_2 nanospheres decorated ZnO NRs as observed in Figure 2.

In order to further confirm the above proposed mechanisms for the induced laser

action, different sizes of SiO_2 nanospheres decorated ZnO NRs have been investigated.

Figures 4.5a and (b) show the emission spectra of the pristine ZnO NRs and ZnO NRs

decorated by 190 nm and 250 nm SiO_2 nanospheres under the same pumping energy.

According to Figure 4.5a, we found that the laser action can still be induced with the

position of lasing peaks centered approximately at 384 nm after the decoration of 190

nm SiO_2 nanospheres. However, according to Figure 4.5b, after the decoration of 250

nm SiO_2 nanospheres, even though there exist several random lasing-like peaks

compared to the pristine VS-ZnO NRs, they are not as pronounced as those of ZnO NRs

decorated with 120 nm and 190 nm SiO_2 nanospheres. To investigate the effects of the
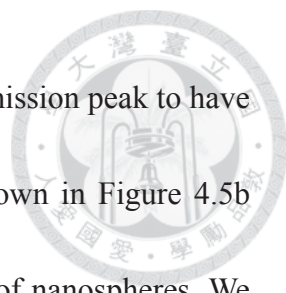
size of decrated SiO_2 nanospheres on the laser action of ZnO NRs, we have examined

the resonant WGMs based on Equation 2. As shown in **Figure 4.6**, it is found that for

the decoration of 190 nm SiO_2 nanospheres, the theoretical TM-resonance peak position

for N=1 is far above 600 nm, which is not in the range of our interest. But, for N=2 the

wavelength of WGM resonance is approximately at 384 nm, which is consistent with

the position of the induced lasing peaks shown in Figure 4.5a. Because of a slight

difference between the peak position of WGM mode and ZnO emission spectrum, there

is a less pronounced enhancement of the lasing action compared to that of the 120 nm

SiO_2 nanospheres decorated ZnO NRs. For the decoration of 250 nm SiO_2 nanospheres,

the nearest theoretical TM-resonance peak position to the ZnO emission spectrum at

389 nm is 378 nm with N=3, which is too far away from the main emission peak to have a significant influence. Therefore, the blurred lasing-like peaks shown in Figure 4.5b can be attributed to the scattering effect induced by the decoration of nanospheres. We thus can see that the random laser action is mainly determined by the condition of WGM resonance. Moreover, the normalized transmittance spectra have been performed for different-size SiO_2 nanospheres with the same number density deposited on glass substrates as shown in **Figure** 4.**7**. It is found that the scattering only has a slight difference among three different-size nanospheres around 389 nm, implying the scattering effect is very similar. It supports the fact that WGM resonance plays a more important role than scattering effect in the induced laser action due to the decoration of SiO_2 nanospheres.

Finally, **Figure 4.8** shows the corresponding CL mapping image for ZnO NRs decorated with 120 nm SiO_2 nanospheres, in which the emission at 389 nm is selected as the mapping wavelength. Compared with the SEM image shown in Figure 4.8a and the CL mapping image shown in Figure 4.8b, it is clear that the bright emission comes from the location where the SiO_2 nanospheres were decorated on ZnO NRs. It therefore provides a firm evidence that SiO_2 nanospheres do play a very important role for the enhancement of light emission and the intensity of 389 nm radiation is indeed amplified by the cavity of SiO_2 nanospheres with WGM resonance.

4.3 Summary

In conclusion, a novel approach to enhance random laser action based on WGM resonance has been demonstrated. It is found that the lasing characteristics can be improved significantly, including narrower emission spectra, sharper lasing peaks, smaller lasing threshold, and higher differential quantum efficiency. Through the variation of the size of decorated nanospheres, CL mapping images, and the theoretical calculation, we have firmly confirmed that the induced laser action in nanospheres decorated ZnO NRs arises from the assistance of WGM resonance. Our approach could be extended to many other composites consisting of nanoparticles and light emitting materials. It therefore can open up a new route for the creation of highly efficient optoelectronic devices.
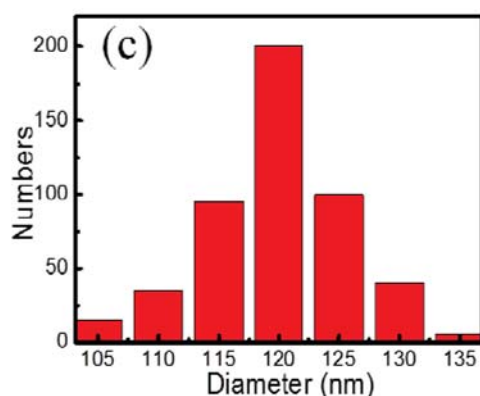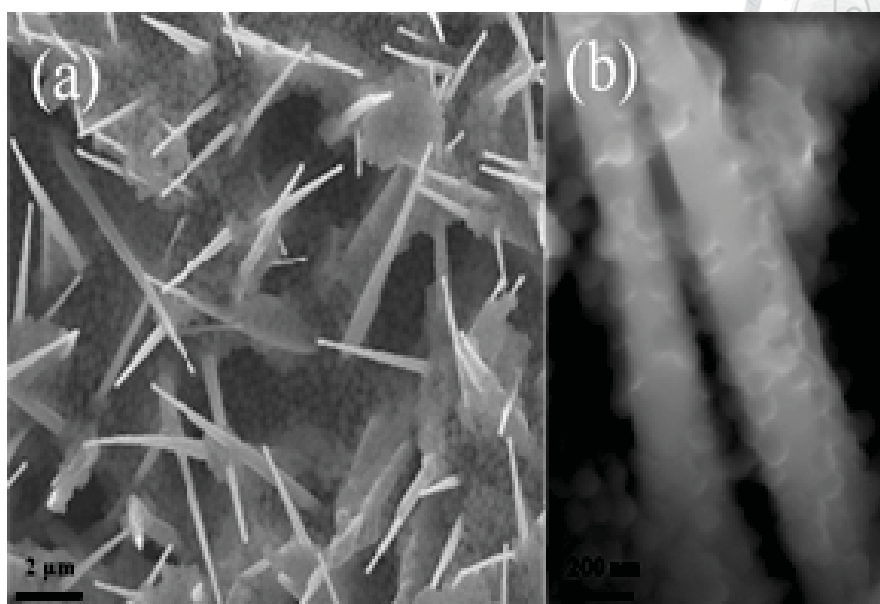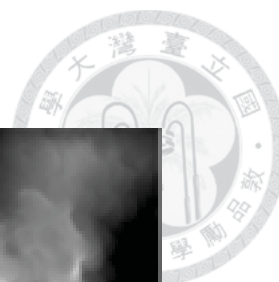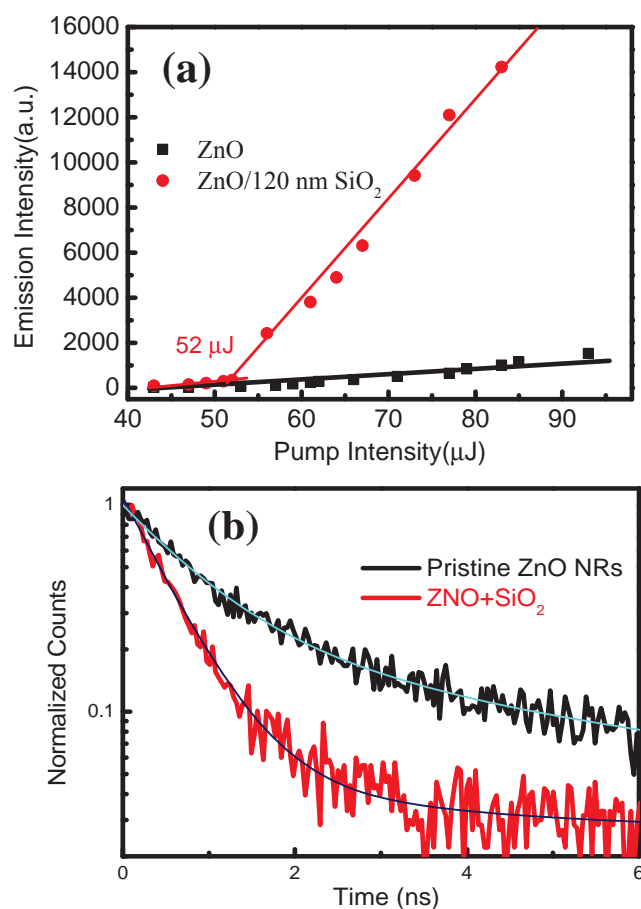
Figure 4.1. (a) Scanning electron microscope image of ZnO nanorods decorated with SiO$_2$ nanospheres. (b) Enlarged SEM image of ZnO nanorods decorated with SiO$_2$ nanospheres. (c) Statistical bar chart of the size distribution of SiO$_2$ nanospheres.
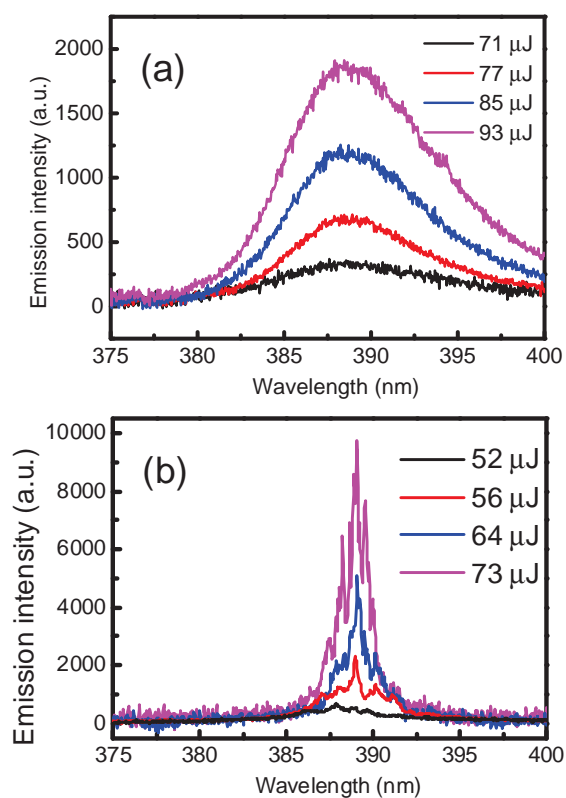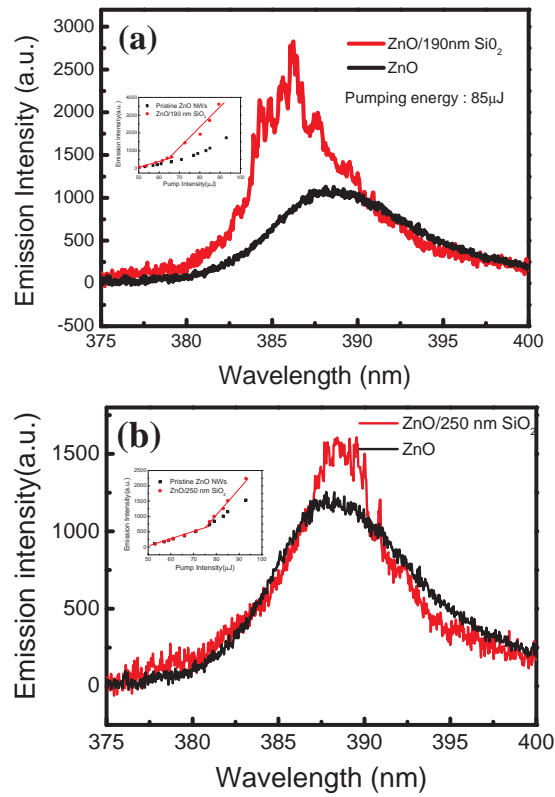
Figure 4.2. (a) and (b) Emission spectra of ZnO nanorods without and with the decoration of 120 nm SiO_2 nanospheres.

Figure 4.3. (a) Plot of the emission intensity versus the pumping energy. Black boxes denote ZnO nanorods and red circles denote pristine ZnO nanorods with the decoration of 120 nm SiO_2 nanospheres. (b) Time-resolved photoluminescence decay spectra with fitting curves for pristine ZnO nanorods and 120 nm SiO_2 nanospheres/ZnO nanorods monitored at the peak emission wavelength of 389 nm.
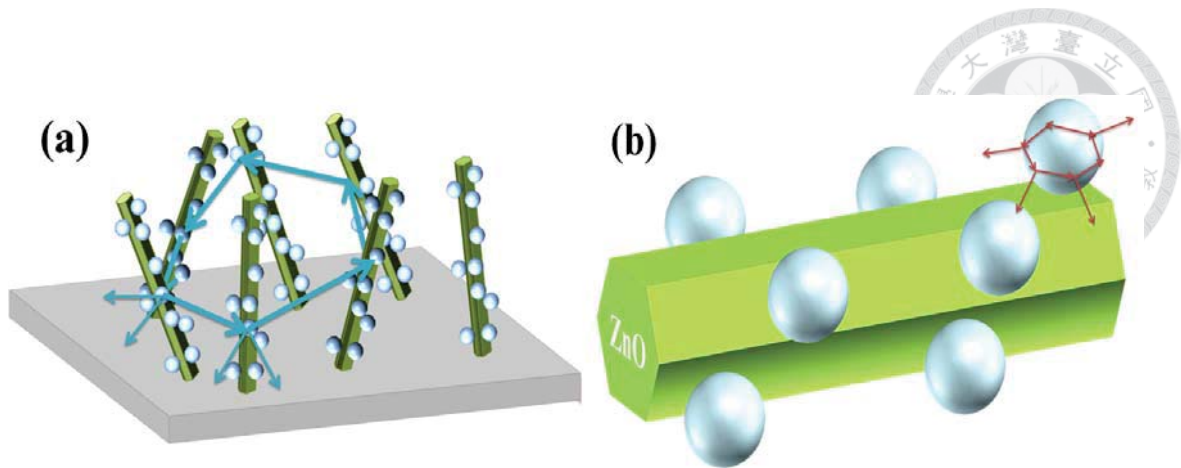
Figure 4.4. Schematic illustration of the mechanisms responsible for the enhanced laser action in SiO_2 nanospheres decorated ZnO nanorods. (a) SiO_2 nanospheres serve as scattering centers to assist light traveling in a randomly closed loop. (b) SiO_2 nanosphere serves as an excellent spherical cavity for the occurrence of whispering gallery made resonance.

Figure 4.5. (a) and (b) Emission spectra of ZnO nanorods without and with the decoration of 190 nm and 250 nm SiO_2 nanospheres under the same excitation power. The insets show plots of the emission intensity versus the pumping energy. Black boxes denote pristine ZnO nanorods and red circles denote ZnO nanorods decorated with the decoration of SiO_2 nanospheres.
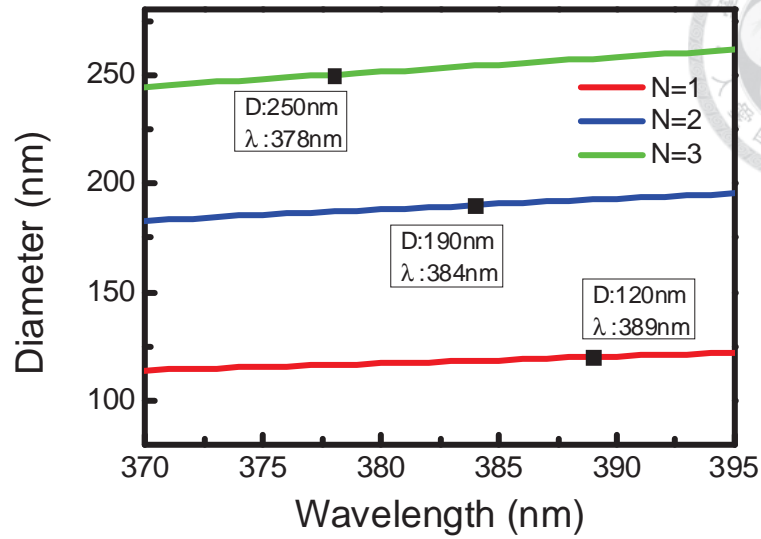
Figure 4.6. Plot of the diameter of spherical cavity versus TM-resonance peaks according to the therotical calculation given by Equation 1. For 120 nm SiO_2 nanospheres, the TM-resonance peak position by the theoretical calculation is approximately at 389 nm for N=1. For 190 nm SiO_2 nanospheres, the theoretical TM-resonance peak position is approximately at 384 nm for N=2 (N=1 is far above 600 nm). And, for 250 nm SiO2 nanospheres, the theoretical TM-resonance peak position is at 378 nm for N=3.
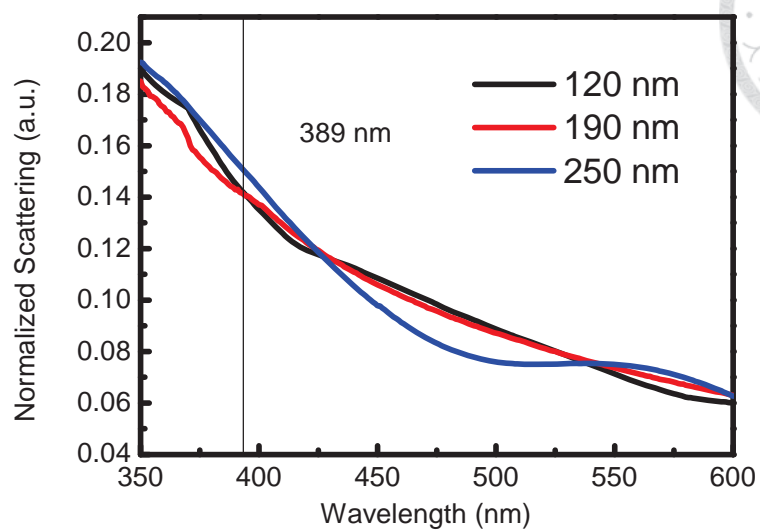
Figure 4.7. Scattering spectra of SiO₂ nanospheres with three different sizes. It is clear that the transmittances for three different-size SiO2 nanospheres around 389 nm only exhibit a slight difference.
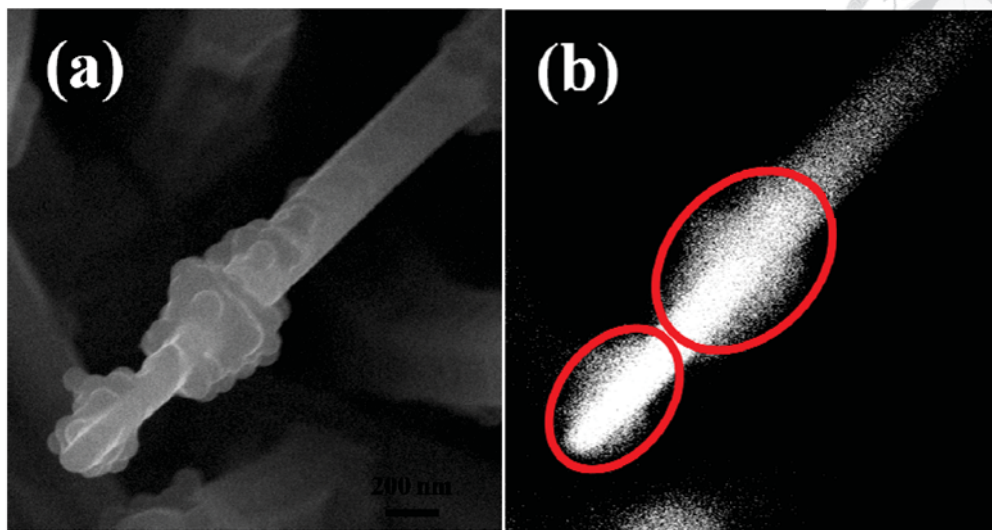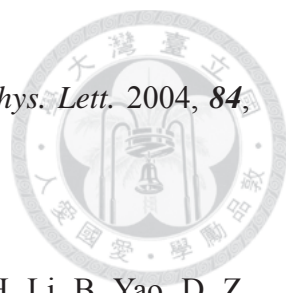
Figure 4.8. (a) Scanning electron microscope image of SiO_2 nanospheres decorated ZnO nanorods. (b) The corresponding cathodoluminescence mapping image.

Reference

1. V. S. Letokhov, *Sov. Phys. JETP* 1968, *26*, 835.

2. B. Q. Sun, M. Gal, Q. Gao, H. H. Tan, C. Jagadish, T. Puzzer, L. Ouyang, and J. Zou, *J. Appl. Phys.* 2003, *93*,5855.

3. F. Quochi, *J. Opt.* 2010, *12*,024003.

4. W. Guerin, N. Mercadier, F. Michaud, D. Brivio, L. S. Froufe-Perez, R. Carminati, V. Eremeev, A. Goetschy, S. E. Skipetrov, and R. Kaiser, *J. Opt.* 2010, *12*,024002.

5. H. Cao, Y. G. Zhao, S. T. Ho, E. W. Seelig, Q. H. Wang, and R. P. H. Chang, *Phys. Rev. Lett.* 1999, *82*, 2278-2281.

6. J. E. Shaw, P. N. Stavrinou, and T. D. Anthopoulos, *Adv. Mater.* 2013, *25*, 552-558.

7. T. S. Kulmala, A. Colli, A. Fasoli, A. Lombardo, S. Haque, and A. C. Ferrari, *ACS Nano* 2011, *5*, 6910–6915.

8. M. L. Lu, T. M. Weng, J. Y. Chen, Y. F. Chen, *NPG Asia Mater.* 2012, *4*, e26.

9. M. Lin. Lu, C. Wei. Lai, H. Ju. Pan, C. T. Chen, P. T. Chou, and Y. F. Chen, *Nano Letters* 2013,   DOI: 10.1021/nl3041367.

10. X. Fang, J. Yan, L. Hu, H. Liu, and P. S. Lee, *Adv. Funct. Mater.* 2010, *22*, 1613-1622.

11. T. Zhai, M. Ye, L. Li, X. Fang, M. Liao, Y. Li, Y. Koide, Y. Bando, and D. Golberg, *Adv. Mater.* 2010, *22*, 4530-4533 (2010).

12. S. F. Yu, C. Yuen, S. P. Lau, W. I. Park, and G. C. Yi, *Appl. Phys. Lett.* 2004, *84*, 3241-3243.

13. H. Zhu, C. X. Shan, J. Y. Zhang, Z. Z. Zhang, D. X. Zhao, B. H. Li, B. Yao, D. Z. Shen, X. W. Fan, Z. K. Tang, X. H. Huo, and K. L. Choy, *Adv. Mater.* 2010, *22*, 1877-1881.

14. A. Tsukazaki, M. Kubota, A. Ohtomo, T. Onuma, K. Ohtani, H. Ohno, S. F. Chichibu, and M. Kawasaki, *Jpn. J. Appl. Phys.* 2005, *44*, L643-L645.

15. S. Chu, M. Olmedo, Z. Yang, J. Kong, and J. Liu, *Appl. Phys. Lett.* 2008, *93*, 181106.

16. C. Zhang, F. Zhang, T. Xia, N. Kumar, J. I. Hahm, J. Liu, Z. L. Wang, and J. Xu, *Opt. Express* 2009, *17*, 7893-7900.

17. M. H. Huang, *Science* 2001, *292*, 1897-1899.

18. D. J. Gargas, M. C. Moore, A. Ni, S. W. Chang, Z. Zhang, S.-L. Chuang, and P. Yang, *ACS Nano* 2010, *4*, 3270-3276.

19. R. Chen, B. Ling, X. W. Sun, and H. D. Sun, *Adv. Mater.* 2011, *23*, 2199-2204.

20. Y. T. Chen and Y. F. Chen, *Opt. Express* 2011, *19*, 8728-8734.

21. C. W. Chen and Y. F. Chen, *Appl. Phys. Lett.* 2007, *90*, 071104.

22. Y. Wu and P. T. Leung, *Phys. Rev. A* 1999, *60*, 630-633.

23. T. J. Lin, H. L. Chen, Y. F. Chen, and S. Cheng, *Appl. Phys. Lett.* 2008, *93*, 223903.

24. I. S. Grudinin, A. B. Matsko, and L. Maleki, *Phys. Rev. Lett.* **2009**, *102*, 043902.

25. A. Umar, S. H. Kim, Y. S. Lee, K. S. Nahm, and Y. B. Hahn, *J. Cryst. Growth* **2005**, *282*, 131-136.

26. M. L. Lu, H. Y. Lin, T. T. Chen, and Y. F. Chen, *Appl. Phys. Lett.* **2011**, *99*, 091106.

27. W. M. Kwok, Y. H. Leung, A. B. Djurišić, W. K. Chan, and D. L. Phillips, *Appl. Phys. Lett.* **2005**, *87*, 093108.

28. A. K. Bhowmik , *Appl. Opt.* **2000** , *39*, 3071.

29. T. Nobis, E. Kaidashev, A. Rahm, M. Lorenz, and M. Grundmann, *Phys. Rev. Lett.* **2004**, *93*, 103903.

Chapter 5

Conclusion

In this thesis, we found that after the decoration of SiO_2 nanospheres, the laser action could be greatly enhanced. Time-resolved photoluminescence experiments have also been performed to verify the enhanced laser action. Through varying SiO_2 nanosphere size, we found that the laser action can be controlled. Morover, by cathodoluminescence apping, theoretical calculation, and scattering, we firmly confirm that wispering-gallery-mode is indeed the underlying mechanism responsible for the enhanced random laser action in SiO_2 nanospheres decorated VS-ZnO NRs. Our result shown here should be very useful for the future development of highly efficient light emitting devices.